

# Analysis of Ionospheric Scintillations using Wideband GPS L1 C/A Signal Data

Todd E. Humphreys, Brent M. Ledvina, Mark L. Psiaki, and Paul M. Kintner, Jr.,  
*Cornell University, Ithaca, N.Y.*

## BIOGRAPHIES

Todd Humphreys is a graduate student in the Sibley School of Mechanical and Aerospace Engineering at Cornell University. He received his B.S. and M.S. in Electrical and Computer Engineering from Utah State University. His research interests are in estimation and filtering, spacecraft attitude determination, GPS technology, and GPS-based study of the ionosphere and neutral atmosphere.

Brent M. Ledvina is a Postdoctoral Associate in the School of Electrical and Computer Engineering at Cornell University. He received a B.S. in Electrical and Computer Engineering from the University of Wisconsin at Madison and a Ph.D. in Electrical and Computer Engineering from Cornell University. His research interests are in the areas of ionospheric physics, space weather, estimation and filtering, and GPS/GNSS technology and applications.

Mark L. Psiaki is an Associate Professor of Mechanical and Aerospace Engineering at Cornell University. He received a B.A. in Physics and M.A. and Ph.D. degrees in Mechanical and Aerospace Engineering from Princeton University. His research interests are in the areas of estimation and filtering, spacecraft attitude and orbit determination, and GPS technology and applications.

Paul Kintner is a Professor of Electrical and Computer Engineering at Cornell University. He received a B.S. in Physics from the University of Rochester and a Ph.D. in Physics from the University of Minnesota. His research interests include the electrical properties of upper atmospheres, space weather, and developing GPS instruments for space science. He is a Fellow of the APS.

## ABSTRACT

A non-real-time GPS receiver has been developed and tested for use in scintillation analysis. The receiver consists of a digital storage receiver and non-real-time software acquisition and tracking algorithms. The goal of this work is to shed light on the behavior of strongly scintillating signals: signals which cause conventional GPS receivers to lose carrier lock.

The receiver collects wideband GPS L1 digital data

sampled at 5.7 MHz using an RF front-end and stores it on disk for post-processing. It processes the data off-line to determine carrier signal amplitude and phase variations during scintillations. The main processing algorithms are traditional code delay and carrier frequency acquisition algorithms and special signal processing algorithms that effectively function as a delay-locked loop and phase-locked loop. The tracking algorithms use non-causal smoothing techniques in order to optimally reconstruct the phase and amplitude variations of a scintillating signal. These techniques are robust against the deep power fades and strong phase fluctuations characteristic of scintillating signals.

To test the receiver, scintillation data were collected in Cauchoeira Paulista, Brazil, from December 4 to 6, 2003. The data set spans several hours and includes times when one or more satellite signals are scintillating. The smoothing algorithm has been used to determine the carrier amplitude and phase time histories of the scintillating signals along with the distortion of the pseudorandom noise (PRN) code's autocorrelation function. These quantities provide a characterization of scintillation that can be used to study the physics of scintillations or to provide off-line test cases to evaluate a tracking algorithm's ability to maintain signal lock during scintillations.

## I. INTRODUCTION

Ionospheric scintillations in radio-frequency (RF) signals passing through the ionosphere were first noted in the 1920s.<sup>1</sup> Since then, they have been the focus of many studies meant to characterize the phenomenon, determine its causes, and investigate its effect on RF communication and navigation systems.<sup>2,3</sup> The advent of the Global Positioning System (GPS) heightened interest in the study of ionospheric scintillations for two reasons. First, the approximately 24 GPS satellites sending RF signals through the ionosphere to thousands of GPS receivers across the globe dramatically increased the density of scintillation-rich signals available for study.<sup>4-9</sup> Second, it was found that ionospheric scintillations could cause loss of tracking lock in GPS receivers, potentially endangering critical GPS applications.<sup>10</sup> There is interest in gaining a better understanding of the effect scintillations have on GPS signal amplitudes and phases in order to better understand

exactly what characteristics of a scintillating GPS signal cause a GPS receiver to lose lock. Such an understanding will facilitate the design of scintillation-robust receivers. Thus, scintillating GPS signals offer data to the scientist and demand savvy from the engineer.

In order to facilitate GPS-based scintillation research, a non-real-time receiver for scintillation analysis has been developed at Cornell University. The Cornell scintillation analysis receiver consists of a digital storage receiver and non-real-time software acquisition/tracking algorithms. The digital storage receiver mixes and filters the incoming L1 coarse/acquisition (C/A) signal to a 2-MHz bandwidth centered at 4.3 MHz. Samples of this wideband signal are stored on disk for post-processing. This process captures wideband L1 C/A data from all the PRN codes available to the receiver regardless of the severity of scintillations affecting the incoming signals. The software tracking algorithm used to post-process the wideband data estimates carrier phase dynamics and signal amplitude over a fixed interval of data using a non-causal estimation technique known as fixed-interval smoothing. Compared to a real-time (causal) estimation algorithm, which relies exclusively on data prior to the time at which an estimate is produced, a smoother exploits data both prior to and posterior to a given estimate, thereby increasing the accuracy of the estimate. This is important for signal tracking during scintillations because inaccuracy in the phase estimate caused by low signal power or strong signal dynamics makes the carrier phase difficult to track.

The scintillation analysis receiver can be compared with real-time scintillation monitors like those of Refs. 4 and 6. The Cornell scintillation monitor presented in Ref. 6 and demonstrated in Ref. 7 is a single-frequency Zarlink/Plessey GPS Builder 2 receiver whose software has been modified to record 50-Hz amplitude and 10-Hz phase measurements. The scintillation monitor presented in Ref. 4 is a modified commercial receiver. It records both amplitude and phase data at 50 Hz. Its carrier tracking bandwidth has been widened to enable tracking through scintillations. Its ability to maintain lock during moderate scintillations has been documented in Ref. 8. Both of these receivers are useful in situations where real-time scintillation monitoring is required (e.g. for GPS integrity monitoring).

The after-the-fact nature of the Cornell scintillation analysis receiver offers two advantages over these receivers. First, by exploiting data prior to and posterior to a given estimate, the smoother-based phase and amplitude estimates produced by the scintillation analysis receiver are more accurate than estimates produced by real-time receivers. Accurate phase and amplitude estimates are important in their own right, but they

also enable tracking through strong scintillations. Second, after-the-fact processing permits enormous flexibility in analyzing the recorded scintillation data. Consider these examples:

- Different tracking algorithms or tuning parameters may be used when post-processing the data.
- Forward-pass loss-of-lock can be bridged by a backward pass after reacquisition.
- The integrated signal power at multiple correlation offsets may be used to investigate multipath-like scintillation effects by calculating the cross-correlation function between the PRN code and the received signal.
- The effects of receiver clock error can be removed from carrier phase estimates.

The Cornell scintillation analysis receiver was used to collect wideband GPS data during strong ionospheric scintillations at Cauchoeira Paulista, Brazil from December 4 to 6, 2003. The real-time receiver of Ref. 6 was co-located with the scintillation analysis receiver to permit a later comparison of the output from each receiver. The co-located receiver lost carrier lock for periods up to 15 s several times during strong scintillations. The scintillation analysis receiver continued to record data during these intervals, and later processed it without loss of signal lock. The carrier phase, Doppler shift, Doppler rate, and signal amplitude estimates produced by the receiver for these intervals are examined in a later section. These quantities contain information about the structure and dynamics of the electron density irregularities in the ionosphere. They are also valuable for testing a GPS receiver's response to scintillations. The amplitude and phase time histories for periods of strong scintillations can be used to reconstruct a series of in-phase ( $I$ ) and quadrature ( $Q$ ) accumulations which are fed to the tracking algorithm of the receiver to be tested. This process facilitates the development of scintillation-robust tracking algorithms.

The aim of this work is four-fold: 1) Develop a non-real-time GPS receiver specially designed to study ionospheric scintillations, 2) Test the receiver on actual scintillating GPS signals, 3) Extract preliminary information about the ionosphere from the receiver products, and 4) Document phase and amplitude time histories that can be used to test the response of a GPS receiver to scintillations.

The Cornell scintillation analysis receiver is described subsequently. Conditions under which the receiver was tested are then defined. Preliminary results and conclusions follow.

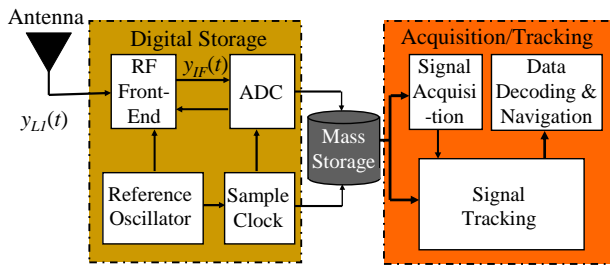


Fig. 1. Block diagram of the Cornell scintillation analysis receiver.

## II. THE SCINTILLATION ANALYSIS RECEIVER

The Cornell scintillation analysis receiver consists of a hardware digital storage receiver and software acquisition/tracking algorithms. Figure 1 presents a functional diagram for the receiver. The received L1 C/A signal is mixed and filtered in the RF front-end, then digitized and stored on disk. It is subsequently retrieved and processed in software. An initial Doppler shift and code delay estimate determined by the signal acquisition algorithm are used to initialize the signal tracking algorithm. In what follows, the digital storage receiver and the acquisition/tracking algorithms are described in detail.

### The Digital Storage Receiver

The digital storage receiver is the hardware component of the scintillation analysis receiver. It is used to record wideband L1 C/A signals for later retrieval and analysis. The principal components of the digital storage receiver are shown in Fig. 2. Its operation is as follows. The incoming GPS L1 signal at 1575.42 MHz is routed to the Zarlink GP2015 RF front-end where it is mixed and filtered in several stages. The mixing frequencies are referenced to a 10 MHz temperature-compensated crystal oscillator (TCXO). In the final mixing/filtering stage the signal is shifted to a center frequency of 4.309 MHz and bandpass filtered to a 2.046 MHz bandwidth. The signal is then sampled at 5.714 MHz using a 2-bit quantization scheme with automatic gain control. Sampling at 5.714 MHz aliases the 4.309 MHz signal to an intermediate frequency (IF) of 1.405 MHz.

The 2-bit sign/magnitude pairs are buffered onto a 32-bit register (not shown in Fig. 2). The contents of the buffer are read in parallel at 357.14 kHz by a data acquisition card connected to a PC. This process requires the PC to read and store data at a rate of 11.43 Mbps. At this rate, a 650 MB compact disk is filled in 7.6 min.

It is important to note that the digitized data recorded by the digital storage receiver contains all the data in a 2-MHz bandwidth about the L1 signal frequency, in-

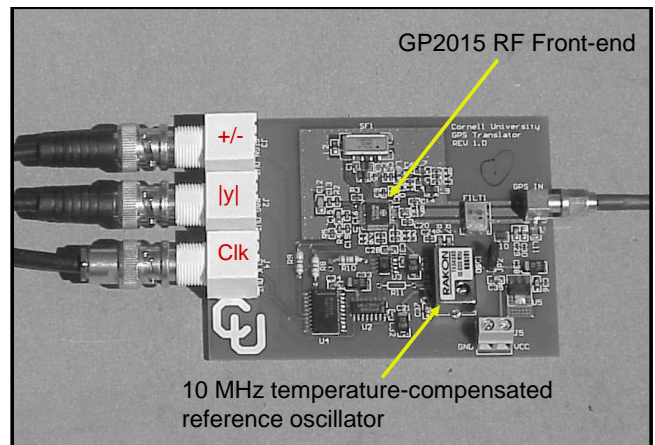


Fig. 2. The digital storage receiver. Outputs are sign (+/-), magnitude ( $|y|$ ), and clock (clk).

cluding PRN codes from each satellite visible to the receiver. These signals may be attenuated or distorted by scintillations, but no data is lost.

It is argued in Ref. 4 that a TCXO is unsuitable for a scintillation receiver because the TCXO's phase instability is on the order of the scintillation-induced carrier phase variations. It will be shown later that the Cornell scintillation analysis receiver's phase estimates were not significantly affected by the TCXO instability. In any case, the after-the-fact nature of the receiver's estimation algorithms allow one to estimate and remove the effects of oscillator instability if necessary by judicious use of carrier phase information from non-scintillating signals.

### Acquisition and Tracking Algorithms

The digitized wideband data is retrieved from storage and processed by software acquisition and tracking algorithms. These are currently implemented in Matlab. The acquisition algorithm is a 2-dimensional search in carrier Doppler shift and code delay. Doppler shift is searched in 25-Hz increments over the range -5250 Hz to 5250 Hz, which corresponds to a maximum radial velocity of 1 km/s. The code delay (code start/stop time) is searched in 1/8-chip increments over the 1-ms PRN code period. The Doppler-shift/code-phase search is carried out using FFT techniques that sum accumulations over 10 code periods.

The software tracking algorithms consist of a smoother-based phase-locked loop (PLL) and a proportional feedback delay-locked loop (DLL) with carrier aiding. The use of the terms *smoother* and *smoothing* in this paper are not to be confused with the concept known as carrier aided smoothing in the GPS literature. In the present context, smoothing refers to an estimation technique called *fixed-interval smoothing*. In this technique,

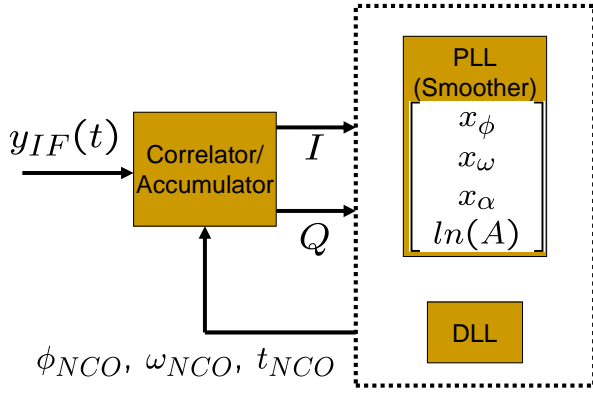


Fig. 3. Block diagram of the software tracking algorithms.

all data gathered over a fixed time interval are used to estimate the state of a system at some time within that interval. A smoother is non-causal in the sense that data prior to and posterior to a given estimate are used to generate that estimate. Because it is non-causal, a smoother cannot be used for real-time estimation, but it is generally more accurate than a real-time estimator.

A smoother uses a system dynamics model to predict the changes in the system state from one time instant to the next. This allows it to incorporate measurements taken while the system state is evolving. The system dynamics model may be nonlinear. The smoother must also include a measurement model to relate measurements at a given time to the system state at that time. The measurement model may also be nonlinear. Finally, the smoother must include a statistical model for the *process noise*, which is the noise affecting the evolution of the state, and the *measurement noise*, which is the noise corrupting the measurements. Inclusion of the process noise distinguishes the smoother from a least-squares batch estimator.

Figure 3 shows a block diagram of the tracking algorithms used in the scintillation analysis receiver. The incoming IF signal  $y_{IF}$  is the L1 signal mixed and aliased to 1.405 MHz by the digital storage receiver. The  $y_{IF}$  signal is mixed to baseband and correlated with a replica of the PRN code to produce  $I$  and  $Q$  accumulations once per code period. The correlator uses the phase ( $\phi_{NCO}$ ) and frequency ( $\omega_{NCO}$ ) estimates produced by the PLL and the code start time estimate ( $t_{NCO}$ ) produced by the DLL. In what follows, an overview of the PLL and DLL will be given. Details of these may be found in Refs. 11 and 12.

To track carrier phase, the smoother-based PLL must estimate carrier phase, Doppler shift, and Doppler rate. It is also useful to estimate the amplitude of the incom-

ing signal. Hence, the smoother's state is chosen as

$$\mathbf{x}_k = [x_\phi, x_\omega, x_\alpha, \ln(A)]_k^T \quad (1)$$

with the following definitions:

$x_{\phi,k} = \phi(t_k) - \phi_{NCO}(t_k)$  : the difference between the true carrier phase and the receiver's numerically controlled oscillator (NCO) phase at time  $t_k$

$x_{\omega,k}$  : the carrier Doppler shift at time  $t_k$

$x_{\alpha,k}$  : the rate of change of the carrier Doppler shift at time  $t_k$

$\ln(A_k)$  : the natural logarithm of the signal's carrier amplitude at time  $t_k$

The smoother's state at time  $t_k$  is related to its state at time  $t_{k+1}$  by the dynamics model

$$\mathbf{x}_{k+1} = \Phi_k \mathbf{x}_k + \mathbf{u}_k + \mathbf{w}_k \quad (2)$$

Here,  $\mathbf{u}_k$  is a control input from the receiver's NCO,  $\omega_{NCO}$ , and  $\mathbf{w}_k$  is the process noise made up by contributions from the receiver clock errors, a random-walk model for line-of-sight/phase scintillation accelerations, and a random walk model for the signal amplitude. Equation (2) includes a discrete-time triple integrator driven by white noise for the update of the phase elements and a random walk model for the carrier amplitude update. The state transition matrix  $\Phi_k$  is given by

$$\Phi_k = \begin{bmatrix} 1 & T_k & \frac{T_k^2}{2} & 0 \\ 0 & 1 & T_k & 0 \\ 0 & 0 & 1 & 0 \\ 0 & 0 & 0 & 1 \end{bmatrix} \quad (3)$$

where  $T_k$  is an accumulation interval. In this case,  $T_k = 1$  ms.

The measurements used by the smoother are the prompt in-phase ( $I$ ) and quadrature ( $Q$ ) accumulations taken over one PRN code interval (1 ms). These are related to the state variables by the following nonlinear measurement model:

$$I_k = \frac{N_k \bar{A}_k d_m}{2} \cos(\Delta\phi_k) + n_{I,k} \quad (4a)$$

$$Q_k = \frac{-N_k \bar{A}_k d_m}{2} \sin(\Delta\phi_k) + n_{Q,k} \quad (4b)$$

with the following definitions:

$I_k$  : the prompt in-phase accumulation for the interval starting at  $t_k$

$Q_k$  : the prompt quadrature accumulation for the interval starting at  $t_k$

$N_k$  : the number of data samples in the accumulation interval

$\bar{A}_k$  : the average signal amplitude over the accumulation interval

$d_m$  : the navigation bit over the accumulation interval (The subscript  $m$  indexes the set of 20 accumulation intervals that constitute the  $m$ th navigation bit interval.)  
 $n_{I,k}$ ,  $n_{Q,k}$  : samples from a zero-mean Gaussian white-noise sequence used to model the noise in the  $I$  and  $Q$  accumulations  
 $\Delta\phi_k = \Delta\phi_k(\mathbf{x}_k, \mathbf{u}_k, \mathbf{w}_k)$  : the average phase error over the accumulation interval

Implicit in Eqs. (4a) and (4b) is the assumption that the receiver DLL is estimating the code delay accurately so that the correlation function  $R(t_{NCO} - t_{TRUE}) \approx 1$ . It is evident from Eqs. (4a) and (4b) that the navigation bits  $d_m$  must be known in order to calculate the  $I_k$  and  $Q_k$  accumulations correctly. The smoother-based PLL addresses this requirement by running two separate estimators in parallel. One estimator propagates the state and performs a measurement update under the assumption that  $d_m = 1$ ; the other estimator does the same under the assumption that  $d_m = -1$ . A Bayesian analysis based on carrier phase and amplitude innovations is used to estimate the relative probabilities of the +1 and -1 navigation data bit signs. These relative probabilities, in turn, are used to synthesize an overall state estimate whose elements are used for the PLL feedback loop, which computes  $\omega_{NCO}$ , and for carrier aiding in the DLL, which computes  $t_{NCO}$ .

The fixed-interval smoother combines an *a priori* state estimate based on the results of the acquisition routine with the  $I_k$  and  $Q_k$  accumulations over a fixed time interval  $\{t_{k_{min}}, t_{k_{min}+1}, t_{k_{min}+2}, \dots, t_{k_{max}}\}$  to estimate the state  $\mathbf{x}_j$  at each  $t_j$  for  $j = k_{min}, \dots, k_{max}$ . The length of the fixed interval is left as a design parameter. In the present study, the smoothing interval is specified to cover periods of interesting scintillation activity. For example, a 25-s smoothing interval over which the collocated scintillation receiver loses phase lock will be examined in detail in a later section. In none of the cases studied did the smoother-based PLL lose carrier lock; but even if it had, the lost segment could probably have been recovered by reacquiring after the lost segment and propagating the signal dynamics backwards. This is a benefit of the after-the-fact nature of the smoother-based PLL.

Note that estimates of  $\mathbf{x}_k$  are produced at 1 kHz. This is much faster than the 50 Hz rates of the receivers presented in Refs. 4 and 6. In most cases the increased time resolution will not be required to reconstruct the dynamics of the electron density irregularities in the ionosphere. These generally have time constants greater than 0.4 s.<sup>6</sup> But if the receiver is used on a low-earth orbiting satellite, the velocity of the ionospheric puncture point increases by approximately 40 times, requiring a



Fig. 4. Test site location in Cachoeira Paulista, Brazil.

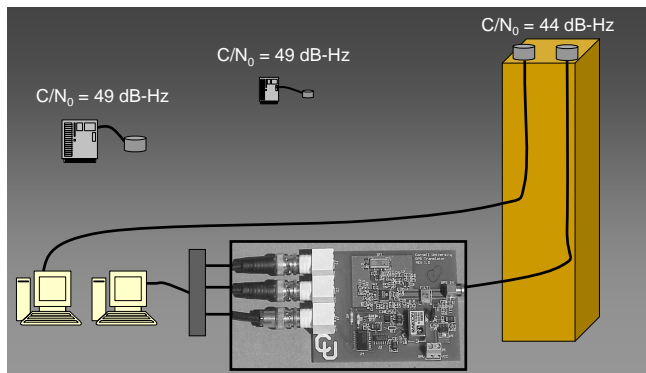


Fig. 5. Experimental setup for testing the scintillation analysis receiver.

sampling rate of 200 Hz to recover significant oscillations from the samples.

The DLL used to track the PRN code start time is a simple zeroth-order proportional feedback controller with discriminator

$$\delta\tau_k = (I_{e,k}^2 + Q_{e,k}^2)^{1/2} - (I_{l,k}^2 + Q_{l,k}^2)^{1/2} \quad (5)$$

where  $I_{e,k}$ ,  $Q_{e,k}$  are the early and  $I_{l,k}$ ,  $Q_{l,k}$  are the late in-phase and quadrature accumulations. The early and late accumulations are separated by 0.5 PRN code chips. The DLL is carrier aided by the Doppler shift estimate produced by the PLL. This enables the DLL to track a ramping Doppler shift.

### III. EXPERIMENTAL SETUP

The Cornell scintillation analysis receiver was tested in Cachoeira Paulista, Brazil from December 4 to 6, 2003. Cachoeira Paulista, shown on the map in Fig. 4, lies along the southern boundary of the equatorial anomaly. This region is notorious for strong ionospheric scintillations. GPS signal amplitude fades of 20 dB are common in the hours following local sunset.

A pictorial representation of the experimental setup used in Cauchoeira Paulista is given in Figure 5. Antennas for the digital storage receiver and a co-located real-time Cornell scintillation monitor (the monitor presented in Ref. 6) were mounted atop a 5-m water tower. Two other real-time Cornell scintillation monitors, identical in functionality to the co-located receiver, were each placed approximately 100 m from the water tower to form a triangular array. The  $I$  and  $Q$  accumulations of the real-time scintillation receivers were later used to validate the carrier amplitude estimates produced by the scintillation analysis receiver.

The data storage device and the co-located receiver were connected to their respective antennas by approximately 20 m of coaxial cable, resulting in a nominal carrier-to-noise ratio of  $C/N_0 = 44$  dB-Hz for strong non-scintillating signals at high elevation. The other two receivers were connected by short 2-m coaxial cables to their antennas, yielding a nominal  $C/N_0 = 49$  dB-Hz. During the 3 nights of testing, the latter two receivers never lost phase lock, presumably owing to their greater carrier-to-noise ratio. In contrast, the co-located receiver lost phase lock frequently when tracking satellites whose signals were experiencing strong scintillations. In most cases, the co-located receiver reacquired carrier phase lock within 1 s, but in other cases it floundered for up to 53 s before reacquiring. In no case did the smoother-based PLL of the scintillation analysis receiver lose lock when post-processing the data recorded by the digital storage receiver. This fact indicates that its forward-pass Kalman filter, which could operate in real time and which is needed in order to eventually do smoothing, would make a good PLL for a real-time receiver.

In all, the data gathered during the campaign in Brazil filled 25 700-MB CDs. These were brought back and processed at Cornell University.

#### IV. RESULTS AND ANALYSIS

Many interesting scintillation events were recorded during the 3-day campaign in Brazil. The results presented here will focus on one such event that occurred just after midnight on December 5, 2003. The event resulted in a 15-s loss of phase lock in the co-located receiver. Figure 6 presents a comparison of the smoothed carrier-to-noise ratio time histories for PRN 7 and PRN 8 during the seconds leading to loss-of-lock in the co-located receiver. At this time, PRN 8 was in the southwest at 45 deg elevation. PRN 7 was nearly directly overhead. The effects of scintillation are evident in the signal from PRN 7;  $C/N_0$  variations of up to 25 dB-Hz occur in the interval shown. In contrast, the  $C/N_0$  ratio for PRN 8 is relatively constant. The smoothed estimates of Doppler

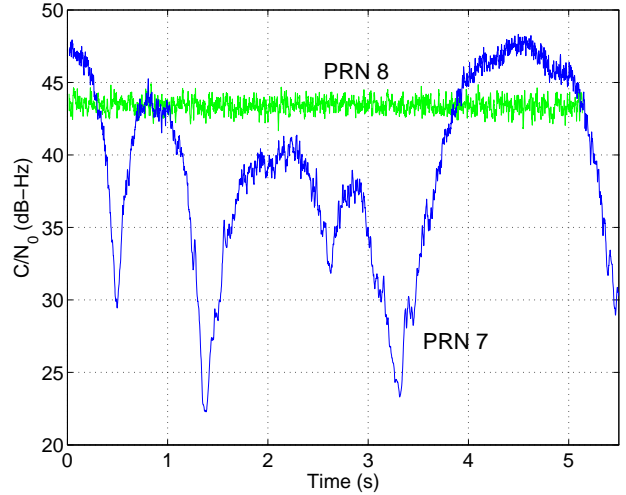


Fig. 6. A comparison of  $C/N_0$  time histories for PRN 7 and PRN 8 on December 5, 2003 which shows the effect of scintillations on PRN 7.

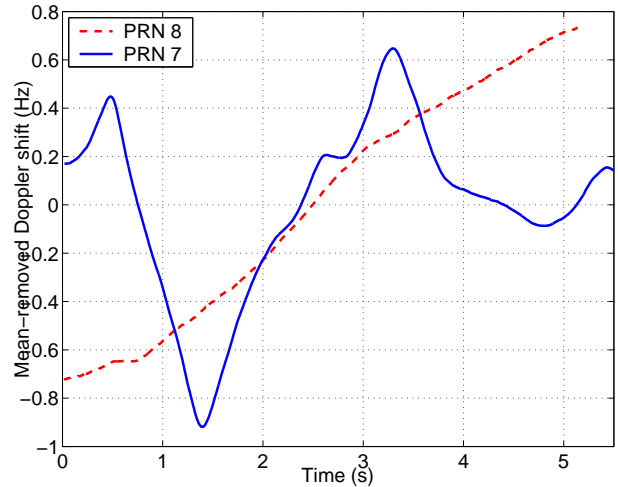


Fig. 7. A comparison of Doppler shift estimates for PRN 7 and PRN 8 for the interval shown in Fig. 6.

shift for PRN 7 and PRN 8 are presented in Fig. 7 for the same interval. The irregularities in the ramping Doppler shift of PRN 8 are due to TCXO instability. These are much smaller than the scintillation-induced variations in the Doppler shift of PRN 7. One can infer from this that the TCXO provides an adequate frequency reference over this interval. If necessary, the effects of TCXO drift could be estimated by subtracting the expected Doppler shift (calculated from GPS satellite ephemerides) from the smoothed Doppler shift estimate for a non-scintillating PRN. The estimated TCXO drift could then be removed from a scintillating Doppler shift estimate, leaving only phase variations caused by scintillations. This possibility illustrates the flexibility of the receiver's after-the-fact processing scheme.

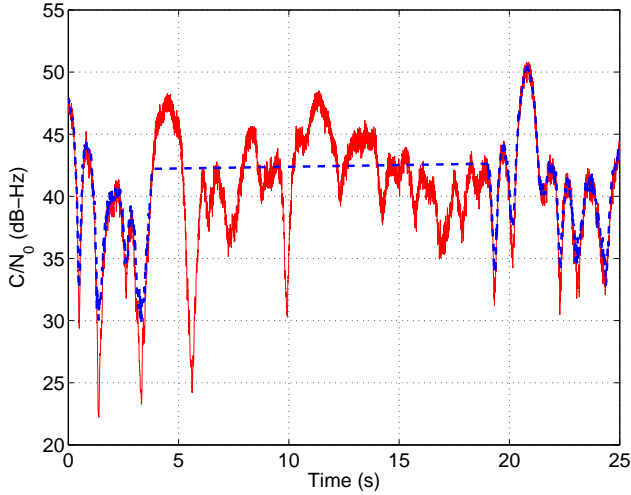


Fig. 8. Loss-of-lock in the co-located receiver (blue dashed line). The smoother-based PLL maintains lock during the same interval (red solid line).

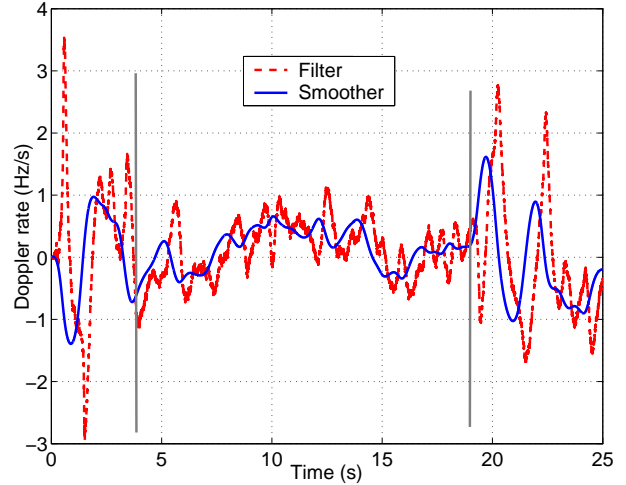


Fig. 10. Filtered and smoothed Doppler rate estimates for the loss-of-lock interval. The vertical gray lines mark the beginning and end of the loss-of-lock experienced by the co-located receiver.

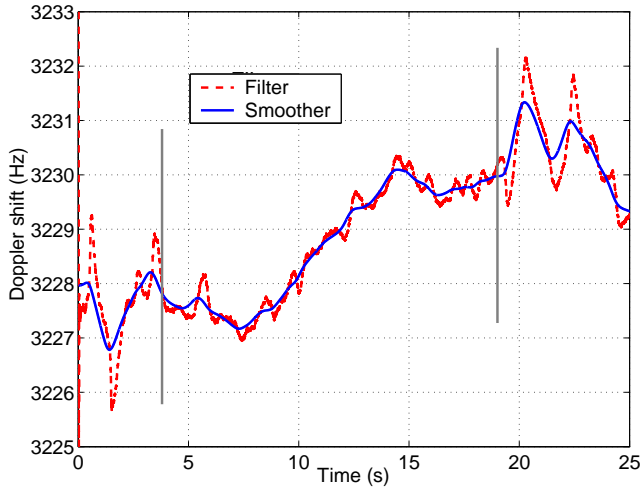


Fig. 9. Filtered and smoothed Doppler shift estimates for the loss-of-lock interval. The vertical gray lines mark the beginning and end of the loss-of-lock experienced by the co-located receiver.

The carrier-to-noise ratio of the co-located receiver is overlaid on the smoothed carrier-to-noise estimate in Fig. 8. The flat line reflects the co-located receiver's loss-of-lock. Thus, the scintillation analysis receiver does not lose lock when the real-time receiver suffers this problem. In addition, a comparison of the power fades in both plots reveals that the co-located receiver tends to underestimate the attenuation caused by scintillations. The carrier Doppler shift estimate (state element  $x_\omega$ ) produced by the smoother-based PLL is presented in Fig. 9. Also shown is the Doppler estimate produced by an extended Kalman filter (EKF) using the same data. The EKF used here employs the same dynamics model, measurement model, and noise models as the smoother. The difference is that the EKF is

causal: it uses only data prior to an estimate to generate that estimate. In Fig. 10 smoothed and filtered estimates for the rate of change of Doppler shift (state element  $x_\alpha$ ) are shown. The vertical gray lines in Figs. 9 and 10 mark the beginning and end of the loss-of-lock experienced by the co-located receiver.

The signal dynamics captured in Figs. 8, 9 and 10 contain information about the dynamics of the electron density irregularities in the ionosphere. For example, the amplitude variations in Fig. 8 contain a sequence of deep fades which likely reflect a pattern of electron density gradients moving across the satellite-to-receiver beam path. Phase scintillations are evident in the Doppler shift and Doppler rate variations of Figs. 9 and 10. Although these contain information about the irregularities that induced them, it is not immediately clear how the variations are related to the irregularities.

One would like to find in Figs. 8-10 some feature linked with the loss-of-lock experienced by the co-located receiver. One might expect, for example, that a radical change in Doppler rate or a deep power fade would immediately precede the loss-of-lock. A close examination of Figs. 8-10 does not present an obvious culprit. Two deep power fades during which  $C/N_0$  drops below 25 dB-Hz do occur in the seconds just before the loss-of-lock, but the loss ultimately takes place at a robust  $C/N_0 = 42$  dB-Hz as the signal rises out of the second power fade. Neither does the smoothed Doppler shift experience any spectacular changes immediately before the loss-of-lock. Perhaps the sudden change of Doppler rate before the loss-of-lock as seen in Fig. 10 is the cause, but this is far from certain. Relying solely on the filtered estimates (red dashed line), one might note

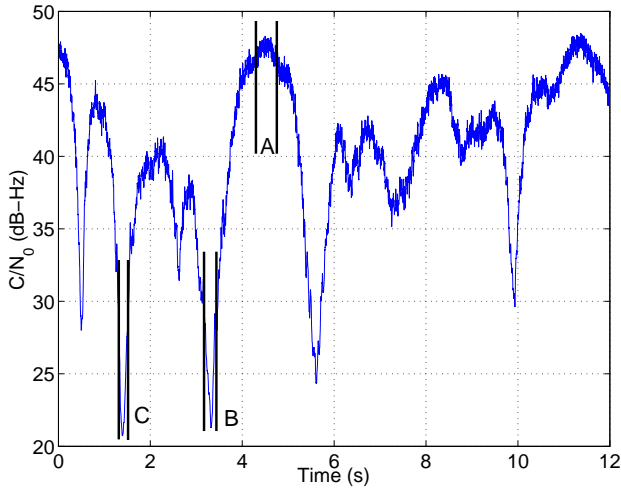


Fig. 11. The first 12 seconds of the loss-of-lock interval with sections to be studied using autocorrelation analysis highlighted.

the peak in Doppler shift and in Doppler rate just before the loss-of-lock and be led to believe that these precipitated the loss; but the smoothed estimates (blue solid line) do not include such large jumps. The smoother was able to fit the estimates to the measurements without such radical changes in Doppler shift and Doppler rate. A close examination of Figs. 8 to 10 reveals that the large excursions in the filtered Doppler shift and Doppler rate estimates line up with the power fades in the  $C/N_0$  plot. This suggests that the magnitudes of the Doppler rate excursions are not realistic, but reflect a loss of phase information as the  $I$  and  $Q$  magnitudes are attenuated during the power fades. In any case, the radical jumps that occur in the filtered estimates before loss-of-lock are exceeded in severity by jumps that occur after reacquisition, and these did not cause further loss-of-lock. Clearly the cause of the loss-of-lock is not immediately evident from the phase and amplitude estimates.

In future studies, the carrier phase and amplitude time histories produced by the smoother will be used to reconstruct  $I$  and  $Q$  time histories. These will be fed to a simulator of the real-time scintillation receiver that lost phase lock to determine whether the loss-of-lock can be re-created. If so, then the tracking loops of the real-time receiver will be examined at the point of loss-of-lock to determine the exact cause of the loss. More broadly, the reconstructed  $I$  and  $Q$  time histories can be used to evaluate the performance of any GPS signal tracking algorithm proposed for use during strong scintillations.

The after-the-fact nature of the scintillation analysis receiver permits other interesting studies of the effects of scintillations. Whereas most receivers produce early, prompt, and late PRN correlations, the correlator of

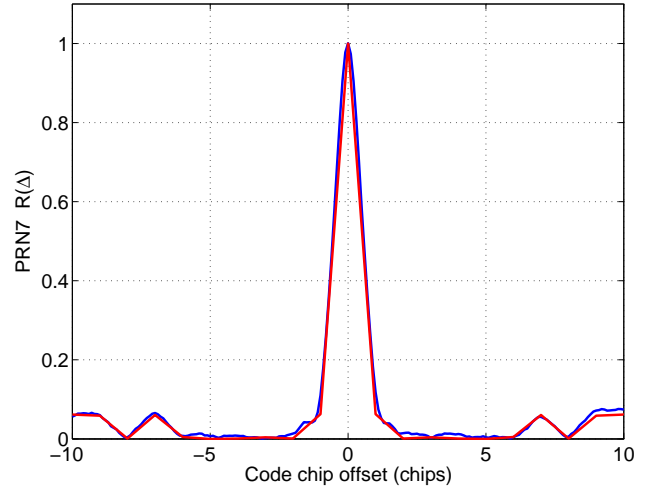


Fig. 12. Cross-correlation of the incoming PRN code and the PRN code replica generated by the scintillation analysis receiver during interval A.

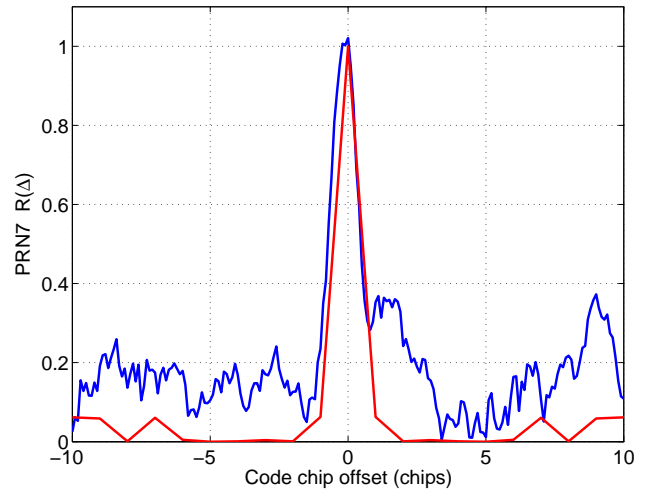


Fig. 13. Cross-correlation of the incoming PRN code and the PRN code replica generated by the scintillation analysis receiver during interval B.

the scintillation analysis receiver can be modified to calculate PRN correlations at any desired offset. This multi-correlator capability has been exploited to study distortion in the PRN autocorrelation function during scintillations. Figure 11 shows the  $C/N_0$  time history for the first 12 s of the loss-of-lock interval studied thus far. Within this interval, a high-power region (A) and two low-power regions (B and C) are marked. Multiple correlations, each at a different offset from the prompt correlation, were averaged over regions A, B, and C to determine the profile of the average autocorrelation function over each region. Each  $I_k$ ,  $Q_k$  pair used to calculate the average is normalized by the estimated signal amplitude  $A_k$ . The resulting autocorrelation profiles are compared to the theoretical autocorre-

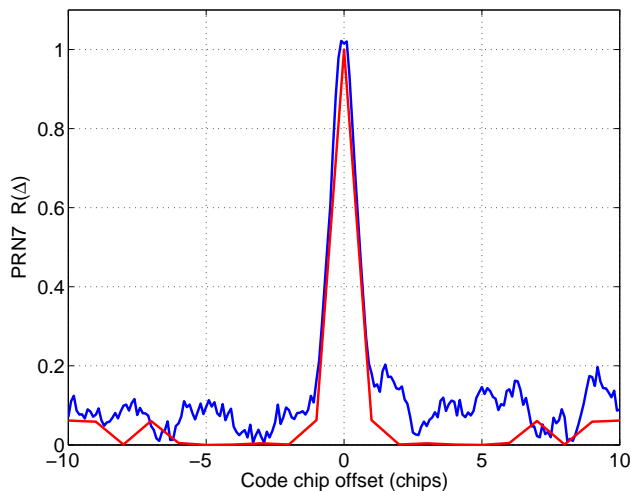


Fig. 14. Cross-correlation of the incoming PRN code and the PRN code replica generated by the scintillation analysis receiver during interval C.

lation function for PRN 7 in Figs. 12-14.

As would be expected for the high  $C/N_0$  level in region A, the reconstructed and theoretical autocorrelation functions agree closely. The higher noise floor in Figs. 13 and 14 reflects the diminished  $C/N_0$  during the power fades in regions B and C. The interesting feature in these two plots is the distortion at approximately 1 PRN chip delay (just to the right of the autocorrelation peak). Such distortion is characteristic of signal multipath. That is, it is characteristic of a weak signal traveling to the receiver along an indirect signal path, arriving approximately 1 PRN chip after the direct signal. One might conjecture that these small bumps are the result of an indirect beam from PRN 7 that has been refracted toward the receiver by a pocket of high electron density, following an indirect path about 300 m longer than the direct path. On the other hand, the two bumps could be the result of typical noise fluctuations. Several other power fades have been studied, some showing signs of multipath and others not. Further study will be required to investigate multipath effects during scintillation in order to determine whether these bumps are just random noise or a multipath-type phenomenon that is associated with ionospheric scintillations. The scintillation analysis receiver makes this kind of study possible. The autocorrelation plots of Figs. 12-14 cannot be generated by existing real-time scintillation receivers.

## V. SUMMARY

A non-real-time scintillation analysis GPS receiver has been developed at Cornell University. The receiver consists of a hardware digital storage receiver and software acquisition/tracking algorithms. It has been used to

record and analyze scintillating L1 C/A signals from Cauchoeira Paulista, Brazil. The receiver's smoother-based tracking algorithm has been used to characterize the carrier phase, Doppler shift, Doppler rate, and carrier amplitude variations associated with scintillations. No obvious causes for loss of carrier phase lock are evident in the phase and amplitude dynamics. The receiver's multi-correlator capability has been used to discover evidence of multipath-like distortion in the autocorrelation function of a PRN code affected by scintillation. The accuracy and flexibility of the receiver cannot be equaled by a real-time scintillation receiver. The scintillation analysis receiver has proved its effectiveness as a tool for studying ionospheric scintillations. The hope is that further useful science will be gleaned from its data products through further analysis and in future applications.

## ACKNOWLEDGMENTS

This work is supported by ONR grant number N00014-92-J-1822 and by the NASA Office of Space Science through grant No. NAG5-12211. David Sibeck is the grant monitor for the latter grant. The authors would like to thank Dr. Eurico R. de Paula of INPE for his collaboration during the data-gathering campaign in Brazil.

## References

- [1] Booker, H. G. and Wells, H. W., "Scatter of radio waves by the F-region of the ionosphere," *Terrestrial Magnetism and Atmospheric Electricity*, Vol. 43, No. 3, 1938, pp. 249–256.
- [2] Yeh, K. C. and Liu, C. H., "Radio wave scintillations in the ionosphere," *Proceedings of the IEEE*, Vol. 70, No. 4, 1982, pp. 324–360.
- [3] Aarons, J., Klobuchar, J. A., Whitney, H. E., Austen, J., Johnson, A. L., and Rino, C. L., "Gigahertz scintillations associated with equatorial patches," *Radio Science*, Vol. 18, No. 3, 1983, pp. 421–434.
- [4] Van Dierendonck, A. J., Klobuchar, J., and Hua, Q., "Ionospheric Scintillation Monitoring Using Commercial Single Frequency C/A Code Receivers," *Proceedings of the 1993 ION GPS Conf.*, Portland, Oregon, 2003, pp. 1333–1342.
- [5] Aarons, J., "Global positioning system phase fluctuations at auroral latitudes," *Journal of Geophysical Research*, Vol. 102, 1997, pp. 17,219.
- [6] Beach, T. L., *Global Positioning System Studies of Equatorial Scintillations*, Ph.D. thesis, Cornell University, Ithaca, N.Y., 1998.
- [7] Beach, T. L. and Kintner, P. M., "Simultaneous Global Positioning System observations of equatorial scintillations and total electron content fluctuations," *Journal of Geophysical Research*, Vol. 104, 1999, pp. 22,553–22,565.
- [8] Van Dierendonck, A. J. and Hua, Q., "Measuring Ionospheric Scintillation Effects from GPS Signals," *Proceedings of the 2001 ION Annual Meeting*, Albuquerque, New Mexico, 2001, pp. 391–396.
- [9] Ledvina, B. M., Makela, J. J., and Kintner, P. M., "First observations of intense GPS L1 amplitude scintillations at midlatitude," *Geophysical Research Letters*, Vol. 29, No. 14, 2002, pp. 4–1–4–4.
- [10] Klobuchar, J. A., "Ionospheric Effects on GPS," *Global Positioning System: Theory and Applications*, edited by B. W. Parkinson and J. J. Spilker, American Institute of Aeronautics and Astronautics, Washington, DC, 1996, pp. 485–515.

- [11] Psiaki, M. L., "Smoother-Based GPS Signal Tracking in a Software Receiver," *Proceedings of the 2001 ION GPS Conf.*, Salt Lake City, Utah, 2001, pp. 2900–2913.
- [12] Psiaki, M. L. and Jung, H., "Extended Kalman Filter Methods for Tracking Weak GPS Signals," *Proceedings of the 2002 ION GPS Conf.*, Portland, Oregon, 2002, pp. 2539–2553.